Title

Organic Matter in Extraterrestrial Water-Bearing Salt Crystals

Authors

Queenie H. S. Chan[1]*†, Michael E. Zolensky[1], Yoko Kebukawa[2], Marc Fries[1], Motoo Ito[3], Andrew Steele[4], Zia Rahman[5], Aiko Nakato[6], A.L. David Kilcoyne[7], Hiroki Suga[8], Yoshio Takahashi[9], Yasuo Takeichi[10,11], Kazuhiko Mase[10,11]

Affiliations

[1]ARES, NASA Johnson Space Center, Houston, Texas 77058, USA

[2]Faculty of Engineering, Yokohama National University, 79-5 Tokiwadai, Hodogayaku, Yokohama 240-8501, Japan

[3]Kochi Institute for Core Sample Research, JAMSTEC, 200 Monobe Otsu, Nankoku, Kochi 783-8502, Japan

[4]Geophysical Laboratory, Carnegie Institution of Washington, 5251 Broad Branch Road, Washington, D.C. 20015, USA

[5]Jacobs – NASA Johnson Space Center, Houston, TX 77058, USA

[6]Graduate School of Science, Kyoto University, Kitashirakawa Oiwake-cho, Sakyo-ku, Kyoto 606-8502, Japan

[7]Advanced Light Source, Lawrence Berkeley National Laboratory, 1 Cyclotron Road, Berkeley, CA 94720, USA

[8]Department of Earth and Planetary Systems Science, Hiroshima University, Kagamiyama, Higashi-Hiroshima, Hiroshima 739-8526, Japan

[9]Department of Earth and Planetary Science, The University of Tokyo, Hongo, Bunkyo-ku, Tokyo 113-0033, Japan

[10]Institute of Materials Structure Science, High-Energy Accelerator Research Organization (KEK), 1-1 Oho, Tsukuba, Ibaraki 305-0801, Japan

[11]Department of Materials Structure Science, SOKENDAI (The Graduate University for Advanced Studies)

*Correspondence to: Queenie H. S. Chan (E-mail: Queenie.Chan@open.ac.uk; Telephone: +1 (585) 653-6144).

†Current address: Department of Physical Sciences, The Open University, Walton Hall, Milton Keynes, MK7 6AA, UK

Abstract

Direct evidence of complex prebiotic chemistry from a water-rich world in the outer solar system is provided by the 4.5-billion-year-old halite crystals hosted in the Zag and Monahans (1998) meteorites. This study offers the first comprehensive organic analysis of the soluble and insoluble organic compounds found in the millimeter-sized halite crystals containing brine inclusions, which sheds light on the nature and activity of aqueous fluids on a primitive parent body. Associated with these trapped brines are organic compounds exhibiting wide chemical variations, representing organic precursors, intermediates and reaction products that include life's precursor molecules such as amino acids, and a mixture of C-, O- and N-bearing materials comprising macromolecular carbon exhibiting a wide range of structural order, aromatic, ketone, imine and/or imidazole compounds. The enrichment in ^{15}N is comparable to the organic matter in pristine CR chondrites, which reflects the source of interstellar ^{15}N such as ammonia and amino acids. The amino acid content of the Zag halite deviates from the meteorite matrix, supporting an exogenic origin of the halite, and therefore the Zag meteorite contains organics synthesized on two distinct parent bodies. Our study suggests that the asteroidal parent body where the halite precipitated, potentially asteroid 1 Ceres, shows evidence for a complex combination of biologically and prebiologically relevant molecules.

One Sentence Summary

Abundant organic compounds were detected in brine-bearing halite crystals originated on a hydrovolcanically-active asteroid.

MAIN TEXT

Introduction

The study of the chemical and organic compositions of ancient (4.5 billion years old (*1-3*)) salt crystals in the Monahans and Zag ordinary chondrites provides key information about the raw materials present in the early solar system, and clues for how solar system dynamics could have facilitated organic redistribution amongst various solar system bodies. Direct samples of early solar system fluids are present in these two ordinary chondrite regolith breccias (Monahans (1998) [H5], hereafter "Monahans" and Zag [H3-6]), which were found to contain brine-bearing halite (NaCl) and sylvite (KCl) crystals (hereafter collectively called "halite") that have been added to the regolith of an S-type asteroid following the latter's thermal metamorphism (*1, 4*) (**Fig. 1**). Halite's typical association with water as an evaporite mineral underscores its importance from the origin and detection of life perspective, in terms of the development of life via offering crystalline surfaces as adsorption sites for catalytic synthesis, concentration, polymerization and organization of prebiotic molecules (*5*). Furthermore, inclusions in halite crystals raise the possibility of trapping life and/or biomolecules from the evaporating aqueous phase (*6*). The brine solutions in Zag and Monahans halite are samples of exogenous liquid water that record primitive aqueous processes on early planetesimals, and the halite hosts of the brines retain clues to the location and timing of the aqueous alteration event and capture an inventory of associated organic species.

Alongside the 1-10 μm-sized fluid inclusions in the halite are solid inclusions that comprise organic solids (*7*) and mineral components that are almost identical to the reported mineralogy of the Ceres regolith, having an affinity to the CM/CI chondrites (*8*) (**Fig. 1**). Furthermore, interpretation of the Dawn mission data for Ceres also suggests the presence of a mixture of chloride salts and water ice (*9*). Ceres is a C-type asteroid located in the middle main asteroid belt (semi-major axis [a] = 2.767 AU, inclination [i] = 9.73 degrees, eccentricity [e] = 0.097) (*10*). Asteroid 6-Hebe, a proposed parent body of H chondrites, is located in the inner asteroid belt (a = 2.426 AU, i = 14.8 degrees, e = 0.203) close to the 3:l motion resonance with Jupiter at 2.50 AU (*11*), and similarities between the orbits of Hebe and Ceres permit exchange of material between these bodies today and possibly in the past (*12*). Solar system dynamics elucidate large-scale mixing of C- and S-type asteroidal bodies and facilitated material exchanges between different asteroidal bodies in the early solar system (*13*). Continuous dynamics influenced by a smaller-scale Yarkovsky–O'Keefe–Radzievskii–Paddack (YORP) effect (*14*, *15*) permitted further fragmentation of smaller materials to ultimately deliver H chondrites to Earth.

Halite easily dissolves under humid conditions, hence only the Monahans and Zag meteorite fragments that were carefully kept in desiccated environments, such as under dry nitrogen in a laboratory, have preserved abundant blue/purple halite crystals (**Fig. 1**). The abundance of surviving halite in Monahans and Zag suggests that the S-type asteroid was mostly anhydrous after the capture of the halite crystals, which is supported by the paucity of hydrous mineral phases in H chondrites (*4, 16*). The host lithologies are H3-6 suggesting significant thermal metamorphism up to 700°C. However, the presence of aqueous fluid inclusions indicates that the halite was formed and maintained at low temperatures (25−50°C) during its entire lifetime or else the fluids would have escaped from the halite (*1*), and thus thermal metamorphism on the S-type asteroid ceased prior to the capture of the halite crystals. These halite crystals are the only available direct samples of a hydrovolcanically active, C-type asteroid, which previous studies have proposed to be asteroid 1 Ceres (*7*, *12*). As the S-type asteroid was unaltered and unheated after the deposition of halite, it preserves a mixture of organic material produced by distinctive synthetic processes on both asteroidal bodies. With the use of two-step laser desorption/laser ionization mass spectrometry (L^2MS), Raman spectroscopy, scanning transmission X-ray microscopy (STXM) utilizing X-ray absorption near edge structure (XANES) spectroscopy, nanoscale secondary ion mass spectrometry (NanoSIMS), and ultra-performance liquid chromatography fluorescence detection and quadrupole time of flight hybrid mass spectrometry (UPLC-FD/QToF-MS) techniques, we analyzed in detail the compositions of the organic solids and the amino acid content of millimeter-size halite crystals hosted in the Monahans and Zag meteorites (<1 vol% of the meteorite).

Results and discussion

A Zag halite crystal was pressed flat onto annealed high-purity gold foils and analyzed with the μ-L^2MS instrument located at NASA's Johnson Space Center, which was optimized to detect aromatic/conjugated organic molecules at the μm-scale and the

subattomole level (1 amol = 10^{-18} mol) (*17*). The µ-L^2MS utilizes separate laser sources to desorb molecules nonthermally from the sample surface as neutral species, and to "soft" ionize selective compounds. Energy in excess of that needed for ionization is transferred to the kinetic energy of the liberated photoelectron, thereby allowing us to detect intact positive molecular ions with virtually no fragmentation (*18*). Ionization with ~10 eV photos covers essentially all organic compounds as their first ionization potentials lie in the range of 5–10 eV. The µ-L^2MS spectra show signatures of low-mass C_5–C_{10} hydrocarbons at around 70–200 atomic mass units (amu) (**Fig. 2**). Each molecular ion in the µ-L^2MS spectra can indicate the presence of different isomers or any molecules with the same molecular mass, hence proper interpretation of the µ-L^2MS spectra relies on the elucidation of perceivable structural patterns indicating functionalities. Sequence of peaks separated by 14 amu in the range of 70–140 amu due to successive addition of methylene (CH_2) groups indicates alkylated derivatives (*19*), suggesting the presence of monounsaturated alkenes. The high signal intensity at 112 amu suggests the presence of octene and other compounds whereas chlorobenzene is a probable candidate, which can be formed by the reaction of oxidants (e.g. Cl_2, SO_2) or brine with benzene. The low abundance of benzene (78 amu) indicates their consumption via chemical reactions to form larger polyaromatic hydrocarbons (PAHs), such as chlorobenzene, naphthalene (128 amu), acenaphthene (154 amu) and fluorene (166 amu). The presence of SO_2 (64 amu) is accompanied by a lower abundance of SO (48 amu) (**Fig. 2**), suggesting a significant proportion of sulfur-containing material on the C-type asteroid. Volatile sulfur and graphitized carbon were both shown to be present on Ceres (*20*). The reaction of sulfur with benzene can produce diphenyl sulfide (186 amu), via synthesis at elevated or low temperatures with the presence of aluminum chloride as catalyst (*21*). Zag halite organics are comprised predominantly of smaller molecules with an absence of larger PAHs that are common in chondritic material (e.g. phenanthrene [178 amu], pyrene [202 amu]) (*22, 23*).

We directly compared the insoluble organic contents of Zag halite, their solid inclusions, and an associated, carbonaceous, halite-bearing clast in Zag (*24*) using Raman spectroscopy. Raman spectra collected on the dark clast in the Zag meteorite show peaks around the ~1,350−1,600 cm^{-1} spectral region which are typical of the first-order defect (D) and graphite (G) bands of carbonaceous materials (**Fig. 3**A). Properties of the Raman bands describe the thermally induced crystalline ordering of macromolecular carbon (MMC) (*25-27*). We used a two-Gaussian peak-fitting model to decompose the peaks so that the results can be comparable to the published data (*28*).

We performed high-resolution Raman imaging on selected Monahans halite residues using a Witec α-scanning near-field optical microscope (SNOM) which has been customized to incorporate confocal Raman spectroscopy imaging. Although the Raman spectra of the halite crystals are featureless in the first-order spectral region, spectra of abundant µm-sized solid inclusions revealed that they consist largely of highly variable organic matter that includes a mixture of poorly ordered MMC and graphitic carbon. Monahans MMC shows variability indicating a complex formation and alteration history (**Fig. 3**B). Spectra collected from Monahans halite show multiple populations of MMC. One subset (pink circle in **Fig. 3**B) show an affinity with CV3-like MMC. Other MMC in

halite residues and Zag matrix (cyan circles) exhibit structural similarity with carbon from CI, CR, CM, and/or CO chondrites. Several points lie along a line trending between crystalline graphite (lower left on **Fig. 3**B) and the other MMC that is best explained by partial amorphization of crystalline graphite, probably by shock (blue arrow) (*28*). The Monahans halite incorporates MMC with a varied and complex formation/alteration history. Raman analysis of Monahans halites also revealed two instances of chloromethane dissolved in the halite matrix adjacent to MMC inclusions (*29*), probably generated by evolution of methane from the MMC via UV photolysis (*30*) coupled with halogenation and partial dissolution in the halite.

We further analyzed the solid inclusions in halites by dissolving a 2 mm Monahans halite crystal in deionized water and concentrating the residues by filtering the solution through a 1 μm mesh filter membrane. We subsampled the halite residues by the focused ion beam (FIB) technique. Preliminary data of the ~100 nm-thick FIB sections obtained by transmission electron microcopy revealed that these grains include MMC similar in structure to CV3 chondrite matrix carbon, aliphatic carbon compounds, olivine of widely varying composition (Fo_{99-59}), high- and low-Ca pyroxene, feldspars, phyllosilicates (mainly saponite), magnetite, sulfides, metal, lepidocrocite (rust), carbonates, diamond, apatite and zeolites (*7*). We further analyzed newly prepared FIB sections by STXM-XANES to locate C-rich areas and investigate the chemical structure of the carbonaceous material. **Fig. 4**A shows a STXM image of the FIB section. C-rich areas were observed in the corresponding carbon map (**Fig. 4**B). Based on the method provided in (*31*), the atomic N/C ratio of the C-rich material is 0.076 ± 0.004, which lies between that of the IOM in primitive CI, CR, and CM chondrites (~0.04) (*32*) and organic cometary samples from the Stardust collection (~0.1) (*31*). The C-XANES spectrum of the C-rich areas (**Fig. 4**C) showed a peak at 285.0 eV (aromatic carbon) and 286.6 eV (ketone [C=O]) but the aliphatic feature was not present (at ~287.3–288.1 eV) (**Fig. 4**D). N-XANES (**Fig. 4**E) showed a small peak at 398.7 eV (imine [C=N]) and 400.3 eV (protonated imine and/or imidazole). The C-XANES of the residue is dominated by aromatic structure with feature indicating O-bearing functional groups, which is comparable to the IOM in typical primitive chondrites (CM/CI/CR)(*33*). There is no 1s-σ* exciton peak (at 291.7 eV) that is indicative of the development of a graphene structure (*34*), which suggests that most of the organic matter did not experience temperatures higher than ~200°C , and significant graphitization did not take place. An observation that marries well with the Raman data shown in **Fig. 3**. Furthermore, some (but not all) organic nanoglobules found in the Murchison meteorite and cometary (Comet Wild 2) particles are known to be dominated by aromatic structure but the ketone (C=O) feature at 286.6 eV is less prominent in these materials when compared to the halite residues (*33*). Hence the organic structure can be explained by a significant abundance of bridging ketones, which indicates a highly primitive nature for the halite residue organics. The wide range of organic features picked up by Raman spectroscopy and STXM-XANES suggest that the organics hosted in the halites are compositionally diverse.

We use the isotopic compositions of the halite residues in Monahans to interpret the synthetic origin of the halite organic residue. We took isotopic images for C, N, H and O with the JAMSTEC NanoSIMS 50L ion microprobe at a spatial resolution of 100 nm (C,

O, N isotopes) and 200 nm (H isotopes) (**Fig. 5**) and the isotopic ratios are listed in **Table 1**. NanoSIMS elemental images are shown in **Fig. 5**B, C, E, F and the O isotopic ratios are plotted on an oxygen 3-isotope diagram (**Fig. 5**I). The NanoSIMS C elemental map shares similar features with the STXM-XANES data. The C-rich area (**Fig. 5B**) is depleted in ^{13}C ($\delta^{13}C$ = –37.6 ‰) and moderately enriched in ^{15}N ($\delta^{15}N$ = +164.5‰). These isotopic characteristics are broadly consistent with that of the IOM in un-weathered CR chondrites and unequilibrated meteorites (*32*), which show typical enrichments in ^{15}N that likely reflect sources of interstellar ^{15}N such as ammonia (*35*) and not terrestrial contamination. High $\delta^{15}N$ values suggest the presence of organic N-compounds such as hydrocarbons and amino acids that are hosts to heavy N (e.g., $\delta^{15}N$ of polar hydrocarbons = +102 ‰; $\delta^{15}N$ of amino acids = +94‰) (*36*). The δD in the C-rich area shows a terrestrial value (+42.5 ± 54.3 ‰). The low δD values contrast with the high δD values of chondritic IOM (e.g., ~600–1,000‰ in CIs and CMs, ~3,000 ‰ in CRs (*32*)). The water on C-type parent bodies is typically D-poor (*37*), therefore the OM synthesized in and/or processed by the D-poor water on Ceres would also be D-depleted. Assuming Ceres had a larger water fraction than CI/CM, the associated OM would have low δD values provided that the time was sufficient for D/H exchange between OM and the D-poor water during a prolonged aqueous event. Alternatively, the low δD values might have been contributed by terrestrial water incorporated during the extraction of the halite residues in the laboratory. However, since halites rapidly dissolve in water, the organic residues were only in contact with the water for a few seconds, thus this contamination is unlikely.

The Dawn Spacecraft at Ceres reported extensive surficial carbonates accompanied by phyllosilicates and ammonium-bearing species, requiring substantial aqueous alteration (*38*). The organic analyses undertaken in this study indicate the presence of a wide range of highly primitive organic compounds with ketone features possibly contributed by organic solids originating from formaldehyde. Insoluble organic matter (or MMC) and amino acids can be synthesized from formaldehyde, glycolaldehyde, and ammonia under hydrous conditions at temperatures as low as 90°C (*39*). Kinetic experiments predict that organic solids could be synthesized on the order of 100 to 10^4 years even at temperatures as low as 0°C (*40*). We envision that similar organic synthetic processes could have occurred on Ceres that synthesized organic solids as well as other crucial biomolecules including amino acids. To investigate the amino acid composition of the halite, we carefully opened a pristinely preserved Zag meteorite stone (~500 g) in a class 10 cleanroom, and subsampled the newly revealed halite crystals (~3 mg, **Fig. 4**C) with handling tools that had been heated in air at 500 °C for 24 h, and studied the amino acid content of the halite and compared this to that of the matrix of the Zag meteorite using the UPLC-FD/QToF-MS technique.

The Zag meteorite is a matrix-supported, regolith breccia composed of H3–4 matrix, H4–5 light-colored metamorphic lithologies, H5–6 silicate-darkened clasts, impact-melt clasts (*4*), and carbonaceous (CI-like) clasts (*24, 41*). The matrix is shocked [stage S3, weakly shocked up to 15 GPa (*4, 42*)] and thermally metamorphosed to 600−950°C (*16*), all predating incorporation of the halite and C chondrite clasts. Although amino acids (e.g. isovaline) have been synthesized in the laboratory under simulated ice/rock impact

conditions (*43*), the low shock level would not have provided sufficient energy for shock-driven organic reactions to occur. The total amino acid distribution and abundance of the matrix (~1,940 parts per billion [ppb]) (**Table S1**) is comparable to other ordinary chondrites (60–3,330 ppb) (*44, 45*) (**Fig. S1, Fig. S2**), and include amino acids (e.g. glycine, α-, β-alanine; **Fig. 6**) that are typical products of the mineral-catalyzed Fischer Tropsch-/Haber Bosch-type (FTT) gas-grain reactions at elevated temperatures (150−700°C) in the presence of CO, H_2, and NH_3 gases and mineral catalysts (*46-48*). The high enantiomeric ratio (D/L ≈ 0.95; i.e. small L-enantiomeric excesses L_{ee} = –9.77–2.31%) of alanine suggest that it is indigenous to the meteorite (**Table S2**). Racemic alanine accompanied by large L_{ee} for glutamic acid have been reported for meteorites exhibiting high degrees of aqueous alteration due to the differences in their solid-solution phase behaviors (*49*). These amino acids could have been synthesized on the S-type asteroid prior to the material exchange between the C- and S-type parent bodies as the latter was maintained at low temperatures (≤50°C) after the deposition of halite crystals and hence the physical conditions would then be unfavorable for FTT reactions to occur.

The abundances of the small straight-chain, amine-terminal (*n*-ω-amino) amino acids (e.g. γ-ABA and EACA) in the Zag matrix are notably lower than the thermally altered meteorites (*48, 50, 51*). While the Zag matrix is γ-ABA and EACA-deficient, the halite is shown to exhibit an opposite trend and is enriched in γ-ABA and EACA (**Table S1**, **Fig. 6**). The total amino acid concentration in halite (~510 ppb) is also significantly lower than the Zag matrix. The striking difference in the amino acid contents between the halite and matrix indicates their separate synthetic origins (**Fig. 6**). This agrees with the Raman imaging and XANES analyses in this study which indicate the presence of organic-rich solid inclusions that are composed of C chondrite-like MMC and other organic compounds with aromatic and ketone structures, which are incongruent to the organic content of the thermally metamorphosed H-type lithology. Also, the halite crystals are hosted as discrete grains (no reaction rims between the halite and surrounding silicate) within an H-chondrite matrix and their mineral inclusions are incompatible with H chondrites (*16*). The continued presence of fluid inclusions in the halite is further evidence that the incorporation of the halites into the H chondrite postdates the metamorphic epoch (*1, 2*). These observations support the hypothesis that the halite is derived from an exogenic source, possibly a hydrovolcanically active C-type parent body (*7, 52*). Our coordinated organic analyses converge into the same conclusion that halite in Zag and Monahans is host to a wide range of organic matter which probably facilitated amino acid synthesis through aqueous alteration on the C-type parent asteroid. The disparities between the amino acid contents between halite in H chondrites and matrix account for material mixing between the two asteroidal bodies, and explain the complex suite of meteoritic organic compositions that can only be contributed by distinctive reaction pathways.

We propose the following sequence of events for Zag and Monahans and its halite. The halite originated from hydrovolcanism on a C-type parent body (probably asteroid 1 Ceres). Insoluble organic matter and amino acids were produced by aqueous alteration in the presence of formaldehyde and ammonia (*39*). The halite formed as surficial evaporate deposits at the end of the hydrothermal activity, approximately 4.5 billion years old (*1-3*),

trapping brines as well as organic and inorganic solids, and other soluble organic compounds. Subsequent large-scale hydrovolcanism had sufficient escape velocity (*53*) to expel surficial halite and some inorganic stones into space. It was probably during surface exposure or inter-asteroidal transit that the halite gained the blue-purple coloration from electrons trapped in anion vacancies through exposure to ionizing radiation, at which time some trapped carbon generated UV-photolysis-derived chloromethane. The halites and other stones were then deposited into the regolith of an S-type parent asteroid (possibly Hebe), which had already experienced thermal metamorphism that yielded its own distinctive suite of amino acids. Regolith evolution buried the halite and associated stones (the latter becoming the CI-like clasts found in Zag and other H chondrites), incorporating them into fine-grained matrix. The meteorite was later stripped from the S-type parent body via a gentle process, possibly by the YORP effect (*14, 15*), for transport to Earth.

Conclusion

The halite crystals and the organic contained within them provide a unique window into the early history of astromaterials and their mobilization across the early solar system. This model describes the brecciated nature of chondrites and elucidates the complex suite of organics which could only be synthesized through individual processes with different physiochemical conditions. The extensive variety of organics hosted in the halite suggests that the original parent asteroid where the halite precipitated, plausibly Ceres, contains a combination of precursor molecules for complex chemical reactions to occur. Furthermore, in the context of understanding moons such as Enceladus and Europa, halite crystals formed from cryovolcanism and ejected into space represent an ideal sample to study prebiotic and possibly biotic processes on these bodies.

Materials and Methods

L^2MS

The μ-L^2MS was used for the detection and identification of organic molecules in lunar samples. The JSC μ-L^2MS instrument is equipped with a vacuum ultraviolet (VUV) ionization source capable of non-resonant single photon soft ionization enabling the *in situ* detection of virtually any organic molecular system at high sensitivity in the sub-attomole range ($>10^{-18}$ mol) and spatial resolution (~5 μm). The generation of coherent VUV radiation is achieved by the nonlinear frequency tripling of the 3rd harmonic (λ 355 nm) of a mode-locked Q-switched picosecond Nd:YAG laser in a Xe–Ar gas cell to produce 118.2 nm (~10.5 eV) radiation. Since the first ionization potentials for nearly all organic molecules lie in the range of 5–10 eV effectively all organic species can be photoionized with 10.5 eV photons.

Raman spectroscopy

The IDP samples were analyzed using a Jobin-Yvon Horiba LabRam HR (800 mm) Raman microprobe at NASA JSC. The excitation source was a 514.53 nm (green) laser. The slit width and the confocal pinhole aperture were set at 150 μm and 400 μm, respectively. The laser beam was focused through a microscope equipped with a 50× objective (short working distance, numerical aperture = 0.75), and the Raman

backscattered light was collected from the same objective. At this magnification and for the laser used, the Raman probe spatial resolution at the analyzed spot was ~0.8 μm, and the laser power at the sample surface was ~60 μW leading to an intensity of approximately 110 $\mu W/\mu m^2$. The spectral range of 100 cm^{-1} to 4000 cm^{-1} includes the first- and second-order Raman bands of carbon. The exposure time for each spectrum was 5s and three accumulations were obtained for each analytical spot to identify and discard spurious signals, such as those from cosmic rays. Spectral peak identification and methods used in the present study were the same as outlined in (*54*). Graphite standards were commercially obtained.

We collected Raman spectra and images of the halite residues using a Witec α-SNOM at the Carnegie Institution of Washington, customized to incorporate confocal Raman spectroscopic imaging. The excitation source is a frequency-doubled solid-state YAG laser (532 nm) operating between 0.3 and 1 mW output power (dependent on objective). Objective lenses used included a ×100 LWD and a 20 LWD with a 50 μm optical fiber acting as the confocal pinhole. For the collection of multispectral images, Raman spectra were collected (0–3600 cm^{-1} using the 600 lines mm^{-1} grating) at each pixel using an integration time of between 1 and 6 s per pixel. The effects of interfering peaks were removed by phase masking routines based on multiple single-peak fits that were compared to standardized mineral spectra. Spectral peak identification and methods used in the present study were the same as outlined in (*55*).

STXM-XANES

C,N-XANES micro-spectroscopy was performed using the STXM at beam line 5.3.2.2 of the Advanced Light Source, Lawrence Berkeley National Laboratory (*56*) and BL-13A of the Photon Factory (PF), High Energy Accelerator Research Organization (KEK) (*57*). Soft X-rays generated by a bending magnet provided a useful photon range spanning from 250 to 780 eV with a photon flux of 10^7 photons s^{-1}. Energy selection was performed with a low-dispersion spherical grating monochromator, affording an energy resolution ($E/\Delta E$) of 5,000; with most of our data taken at an energy resolution of ~3,000, i.e., at ~0.1 eV. Beam focusing utilized Fresnel zone plate optics for a theoretical spot size of 31 nm. The BL-13A of the PF is an APPLE-II-undulator-based beamline covering photon energies of 50 – 2000 eV with variable polarization. A variable-included-angle Monk-Gillieson mounting monochromator with varied-line-spacing plane gratings is used to achieve a high photon flux of 10^{11} photons/s with a high resolution ($E/\Delta E$) of 10,000 at 400 eV. The spatial resolution of the compact STXM in BL-13A is about 40 nm and the photon intensity at the sample is 10^7 photons/s (*58*). Most of our data were obtained at $E/\Delta E$ of ~3,000.

The C,N-XANES spectra were acquired using a multi-spectral imaging method (‘‘Stacks” method; (*59*)). For C-XANES, in the fine structure portions of the near-edge region (283–295.5 eV), the energy step size (ΔE) was 0.1 eV; in the less featured pre-edge (280–283 eV) and post-edge (295.5–301.0 eV) regions, ΔE was 0.5 eV; in the extended X-ray absorption fine structure (EXAFS) region (301–310 eV), ΔE was 1 eV. For N-XANES, in the fine structure portions of the near-edge region (395–406 eV), ΔE was 0.2 eV; in the less featured pre-edge (385–395 eV) and post-edge (406–410 eV) regions, ΔE was 0.5 eV; in the EXAFS (410–430 eV) region, ΔE was 2 eV. The acquisition time per energy step varied from 3 to 5 ms.

NanoSIMS analysis

The H, C, O and N isotopic compositions of the samples were analyzed by isotopic imaging with the JAMSTEC NanoSIMS 50L ion microprobe (Ametek CAMECA, Inc., Gennevilliers Cedex, France). A focused primary Cs^+ beam of approximately ~1.6 pA for C, O and N isotopic analysis and 4 pA for H isotopic analysis was rastered over 10 × 10 μm^2 areas on the samples. For C, O and N isotopic analysis, images of $^{12}C^-$, $^{13}C^-$, $^{16}O^-$, $^{17}O^-$, $^{18}O^-$ $^{12}C^{14}N^-$, and $^{12}C^{15}N^-$ were acquired simultaneously in multidetection with seven electron multipliers (EMs) at a mass resolving power of approximately 9,500, sufficient to separate all relevant isobaric interferences (i.e., $^{12}C^1H$ on ^{13}C and ^{16}OH on ^{17}O). For H isotopic analysis, images of ^1H, ^2D and $^{12}C^-$ were acquired using three EMs in multidetection at a mass resolving power of approximately 3,000. Each run was initiated after stabilization of the secondary ion beam intensity following presputtering of approximately < 2 min with a relatively strong primary ion beam current (~20 pA). Each imaging run was repeatedly scanned (10 – 20 times) over the same area, with individual images consisting of 256 × 256 pixels. The dwell times were 5,000 μs/pixel for C, O and N isotopic measurements (Total acquisition time ~ 55 min.) and 5,000 μs/pixel for H isotopic measurement (Total acquisition time ~ 110 min.). The isotopic images were processed using the custom written software 'NASA JSC imaging software for NanoSIMS' developed in the Interactive Data Language (IDL) program (*60*).

Nearby grains of 1-hydroxybenzotriazole hydrate with known isotopic compositions of H, C, O and N were used for standards to correct for instrumental mass fractionations [45]. Isotopic compositions are reported as δ values, representing the deviation of the measured isotopic ratios with reference terrestrial standards in per mil (‰):

$$\delta R = \left[\frac{R_{measured}}{R_{reference}} - 1\right] \times 1{,}000$$

Reference values for H, C, and N isotopic ratios are 0.00015576 for D/H ratio of the standard mean ocean water ($SMOW_)$ (*61*), 0.0112372 for the $^{13}C/^{12}C$ ratio of the PeeDee Belemnite (PDB) standards (*62*), and 0.003676 for $(^{15}N/^{14}N)_{Air}$ (*63*).

Amino acid analysis with UPLC-FD/QToF-MS

We analyzed the Zag meteorite provided by E. Thompson. The meteorite sample (selected from the matrix) was powdered and transferred to individual glass ampoules in a Class 100 Labconco laminar flow hood under HEPA-filtered positive pressure. Halite crystals were subsampled from the meteorite with pre-sterilized tools in a Class 10 clean lab at NASA JSC. Sterilized (500°C, 24 h) laboratory halite and alumina samples were subjected to the same procedures and analyzed as procedural blanks.

Porcelain mortars and pestles were scrubbed and washed with dilute soap solution, rinsed with Millipore Integral 10 UV (18.2 MΩ cm, <3 parts-per-billion [ppb] total organic carbon) ultrapure water, hereafter referred to as water, immersed in 20% citric acid and sonicated at room temperature for 60 min. All tools, glassware, and ceramics were rinsed with water, wrapped in aluminum foil, and sterilized by heating in air at 500

°C for 24 h. Volumetric flasks were only rinsed with copious water. Amino acid standards and other laboratory chemicals such as ammonium hydroxide (NH_4OH) (28–30 wt %), sodium hydroxide (NaOH), hydrochloric acid (HCl) (37 %), methanol, hydrazine monohydrochloride, *o*-phthaldialdehyde (OPA), *N*-acetyl-L-cysteine (NAC) were purchased from Fischer Scientific, Sigma-Aldrich, or Acros Organics. Poly-Prep® prepacked ion exchange columns (AG 50W-X8 resin, 200–400 mesh, hydrogen form) were purchased from Bio-Rad. Solutions of sodium borate were prepared from solid sodium tetraborate decahydrate (Sigma Ultra 99.5–100% purity) that was heated in air at 500 °C for 24 h prior to dissolution in water. Amino acid standard solutions were made by dissolving individual amino acid solutes in water, and were combined into a standard mixture analyzed by ultra-performance liquid chromatography fluorescence detection and quadrupole time of flight hybrid mass spectrometry (UPLC-FD/QToF-MS) on a daily basis.

One mL of water was added to each glass ampoule containing separate samples, and the ampoules were flame-sealed and heated to 100 °C for 24 h in an oven. After the hot water extraction, the samples were cooled to room temperature and centrifuged for 5 min to separate water supernatant from solid particulate. Exactly half of the water supernatant (500 μL) was transferred to small test tube (10 × 75 mm), dried under vacuum (Savant™ SPD131DDA SpeedVac™ Concentrator), flame-sealed in a larger test tube (20 × 150 mm) containing 6 N HCl, and then subjected to acid vapor hydrolysis for 3 h at 150 °C in order to liberate amino acids in bound or precursor forms. After the vapor-hydrolysis procedure, the test tubes were rinsed with water, and the bottom of the test tubes were opened to retrieve the inner small test tubes, and this portion of the sample is hereafter referred to as the “hydrolyzed extract”, representing the total amino acid contents of the samples. The remaining hot-water extract was rinsed with 2 × 1 mL water and the supernatant was transferred to individual test tubes, this portion of the sample is hereafter referred to as the “non-hydrolyzed extract”, containing only the free amino acids. Both hydrolyzed and non-hydrolyzed samples were then bought up in 3 × 1 mL of water and desalted on a cation exchange resin. Amino acids were eluted with 2 × 3.5 mL of 2 M NH_4OH. The eluates were collected in small test tubes and evaporated to dryness. The samples were transferred to small sample vials, re-dissolved in 100 μL of water, and stored at −20°C. Immediately before UPLC-FD/QToF-MS analysis, the samples were derivatized with OPA/NAC fluorescent derivatization (*64*). 25 μL of the thawed sample was dried under vacuum, re-suspended in 20 μL 0.1 M sodium borate buffer (pH 9), and derivatized with 5 μL OPA/NAC in 1 mL autosampler glass vials. The derivatization reaction was then quenched after 15 min. at room temperature with 75 μL of 0.1 M hydrazine hydrate.

The amino acid abundances and distributions were measured by UPLC-FD/QToF-MS at NASA JSC, using a Waters ACQUITY ultrahigh performance LC and a Waters ACQUITY fluorescence detector connected in series to a Waters LCT Premier ToF-MS. 25 μL of the derivatized samples were separated using a Waters BEH C18 column (2.1 × 50 mm, 1.7 μm particle size) followed by a second Waters BEH phenyl column (2.1 × 150 mm, 1.7 μm particle size). Chromatographic conditions were: column temperature, 30°C; flow rate, 150 μL min^{-1}; solvent A (50 mM ammonium formate, 8% methanol, pH

8.0); solvent B (methanol); gradient, time in minutes (%B): 0 (0), 35 (55), 45 (100). The electrospray and mass spectrometer conditions have been described by Glavin et al. (*64*). Amino acids in meteorite bulk, halite and control samples were identified by correlating sample compounds with known standards using the representative masses and fluorescence responses of the OPA/NAC amino acid derivatives at the expected chromatographic retention times.

H2: Supplementary Materials

Supplementary material for this article is available at
http://advances.sciencemag.org/cgi/content/full/4/1/eaao3521/DC1

Fig. S1. The 4–40 min region of the UPLC-FD chromatograms obtained for the OPA/NAC labeled (15 min derivatization) 6 M HCl acid-hydrolyzed amino acid extract and the non-hydrolyzed amino acid extract of the Zag matrix, acid-hydrolyzed amino acid extract of the Zag halite, and the amino acid standard solution.
Fig. S2. An overview of the amino acid compositions of Zag matrix and halite compared to chondrites from different meteorite classes.
Fig. S3. C-XANES spectra used to compose false color map in Fig. 4C.
Fig. S4. Representative UPLC-ToF-MS combined ion chromatograms of selected masses.
Fig. S5. Representative UPLC-ToF-MS ion chromatograms.
Table S1. Summary of the average blank-corrected amino acid abundances (in ppb by weight).
Table S2. Amino acid enantiomeric ratios (D/L) of the 6 M HCl acid-hydrolyzed amino acid extract (total) and the non-hydrolyzed amino acid extract (free) of the Zag matrix, acid-hydrolyzed amino acid extract of the Zag halite.*

References and Notes

1. M. E. Zolensky *et al.*, Asteroidal Water Within Fluid Inclusion-Bearing Halite in an H5 Chondrite, Monahans (1998). *Science* **285**, 1377-1379 (1999).
2. J. Whitby, R. Burgess, G. Turner, J. Gilmour, J. Bridges, Extinct 129I in Halite from a Primitive Meteorite: Evidence for Evaporite Formation in the Early Solar System. *Science* **288**, 1819-1821 (2000).
3. D. D. Bogard, D. H. Garrison, J. Masarik, The Monahans chondrite and halite: Argon-39/argon-40 age, solar gases, cosmic-ray exposure ages, and parent body regolith neutron flux and thickness. *Meteoritics & Planetary Science* **36**, 107-122 (2001).
4. A. E. Rubin, M. E. Zolensky, R. J. Bodnar, The halite-bearing Zag and Monahans (1998) meteorite breccias: Shock metamorphism, thermal metamorphism and aqueous alteration on the H-chondrite parent body. *Meteoritics & Planetary Science* **37**, 125-141 (2002).
5. S. W. Squyres *et al.*, In Situ Evidence for an Ancient Aqueous Environment at Meridiani Planum, Mars. *Science* **306**, 1709-1714 (2004).
6. L. J. Rothschild, R. L. Mancinelli, Life in extreme environments. *Nature* **409**, 1092-1101 (2001).

7. M. Fries, M. Zolensky, A. Steele, Mineral inclusions in Monahans and Zag halites: Evidence of the originating body. *Meteoritics and Planetary Science Supplement* **74**, 5390 (2011).
8. H. McSween, J. Castillo-Rogez, J. Emery, M. De Sanctis, in *Lunar and Planetary Science Conference*. (2016), vol. 47, pp. 1258.
9. O. Ruesch *et al.*, Cryovolcanism on Ceres. *Science* **353**, (2016).
10. T. B. McCord, C. Sotin, Ceres: Evolution and current state. *Journal of Geophysical Research: Planets* **110**, n/a-n/a (2005).
11. M. J. Gaffey, S. L. Gilbert, Asteroid 6 Hebe: The probable parent body of the H-type ordinary chondrites and the IIE iron meteorites. *Meteoritics & Planetary Science* **33**, 1281-1295 (1998).
12. M. Fries, S. Messenger, A. Steele, M. Zolensky, paper presented at the 76th Annual Meeting of the Meteoritical Society, Edmonton, Canada, July 29-August 7, 2013 2013.
13. F. E. DeMeo, B. Carry, Solar System evolution from compositional mapping of the asteroid belt. *Nature* **505**, 629-634 (2014).
14. S. C. Lowry *et al.*, Direct Detection of the Asteroidal YORP Effect. *Science* **316**, 272-274 (2007).
15. W. F. Bottke, D. Vokrouhlický, M. Brož, D. Nesvorný, A. Morbidelli, Dynamical Spreading of Asteroid Families by the Yarkovsky Effect. *Science* **294**, 1693-1696 (2001).
16. J. C. Bridges, D. A. Banks, M. Smith, M. M. Grady, Halite and stable chlorine isotopes in the Zag H3–6 breccia. *Meteoritics & Planetary Science* **39**, 657-666 (2004).
17. S. J. Clemett, R. N. Zare, Microprobe two-step laser mass spectrometry as an analytical tool for meteoritic samples. *Symposium - International Astronomical Union* **178**, 305-320 (1997).
18. S. J. Clemett, S. A. Sandford, K. Nakamura-Messenger, F. HÖRz, D. S. McKay, Complex aromatic hydrocarbons in Stardust samples collected from comet 81P/Wild 2. *Meteoritics & Planetary Science* **45**, 701-722 (2010).
19. S. J. Clemett, C. R. Maechling, R. N. Zare, P. D. Swan, R. M. Walker, Identification of Complex Aromatic Molecules in Individual Interplanetary Dust Particles. *Science* **262**, 721-725 (1993).
20. A. R. Hendrix, F. Vilas, J.-Y. Li, Ceres: Sulfur deposits and graphitized carbon. *Geophysical Research Letters* **43**, 8920-8927 (2016).
21. H. B. Glass, E. E. Reid, The direct introduction of sulfur into aromatic hydrocarbons. *Journal of the American Chemical Society* **51**, 3428-3430 (1929).
22. S. Messenger *et al.*, Indigenous Polycyclic Aromatic Hydrocarbons in Circumstellar Graphite Grains from Primitive Meteorites. *The Astrophysical Journal* **502**, 284 (1998).
23. S. Clemett, C. Maechling, R. Zare, C. Alexander, in *Lunar and Planetary Science Conference*. (1992), vol. 23.
24. M. Zolensky *et al.*, in *78th Annual Meeting of the Meteoritical Society*. (2015), vol. 1856, pp. 5270.
25. A. C. Ferrari, J. Robertson, Interpretation of Raman spectra of disordered and amorphous carbon. *Physical Review B* **61**, 14095-14107 (2000).
26. M. Fries, R. Bhartia, A. Steele, in *Lunar and Planetary Science Conference*. (2011), vol. 42, pp. 1860.
27. F. Tuinstra, J. L. Koenig, Raman Spectrum of Graphite. *The Journal of Chemical Physics* **53**, 1126-1130 (1970).

28. M. Fries, M. Burchell, A. Kearsley, A. Steele, Capture effects in carbonaceous material: A Stardust analogue study. *Meteoritics & Planetary Science* **44**, 1465-1474 (2009).
29. M. D. Fries, A. Steele, M. Zolensky, Halogen-substituted methane in Monahans halite. *Meteoritics and Planetary Science Supplement* **75**, 5381 (2012).
30. A. C. Schuerger, J. E. Moores, C. A. Clausen, N. G. Barlow, D. T. Britt, Methane from UV-irradiated carbonaceous chondrites under simulated Martian conditions. *Journal of Geophysical Research: Planets* **117**, n/a-n/a (2012).
31. G. D. Cody *et al.*, Quantitative organic and light-element analysis of comet 81P/Wild 2 particles using C-, N-, and O-μ-XANES. *Meteoritics & Planetary Science* **43**, 353-365 (2008).
32. C. M. O. D. Alexander, M. L. Fogel, H. Yabuta, G. D. Cody, The origin and evolution of chondrites recorded in the elemental and isotopic compositions of their macromolecular organic matter. *Geochimica et Cosmochimica Acta* **71**, 4380-4403 (2007).
33. B. T. D e Gregorio *et al.*, Isotopic and chemical variation of organic nanoglobules in primitive meteorites. *Meteoritics & Planetary Science* **48**, 904-928 (2013).
34. G. D. Cody *et al.*, Organic thermometry for chondritic parent bodies. *Earth and Planetary Science Letters* **272**, 446-455 (2008).
35. G. Cody, C. Alexander, in *Lunar and Planetary Science Conference*. (2017), vol. 48.
36. S. Pizzarello, X. Feng, S. Epstein, J. R. Cronin, Isotopic analyses of nitrogenous compounds from the Murchison meteorite: Ammonia, amines, amino acids, and polar hydrocarbons. *Geochimica et Cosmochimica Acta* **58**, 5579-5587 (1994).
37. C. M. O. D. Alexander *et al.*, The Provenances of Asteroids, and Their Contributions to the Volatile Inventories of the Terrestrial Planets. *Science* **337**, 721-723 (2012).
38. M. C. De Sanctis *et al.*, Bright carbonate deposits as evidence of aqueous alteration on (1) Ceres. *Nature* **536**, 54-57 (2016).
39. Y. Kebukawa, Q. H. S. Chan, S. Tachibana, K. Kobayashi, M. E. Zolensky, One-pot synthesis of amino acid precursors with insoluble organic matter in planetesimals with aqueous activity. *Science Advances* **3**, (2017).
40. Y. Kebukawa, G. D. Cody, A kinetic study of the formation of organic solids from formaldehyde: Implications for the origin of extraterrestrial organic solids in primitive Solar System objects. *Icarus* **248**, 412-423 (2015).
41. M. Zolensky, R. Clayton, T. Mayeda, J. Chokai, O. Norton, Carbonaceous chondrite clasts in the halite-bearing H5 chondrite Zag. *Meteoritics and Planetary Science Supplement* **38**, 5216 (2003).
42. D. Stöffler, K. Keil, S. Edward R.D, Shock metamorphism of ordinary chondrites. *Geochimica et Cosmochimica Acta* **55**, 3845-3867 (1991).
43. Z. Martins, M. C. Price, N. Goldman, M. A. Sephton, M. J. Burchell, Shock synthesis of amino acids from impacting cometary and icy planet surface analogues. *Nature Geoscience*, (2013).
44. Z. Martins *et al.*, Amino acid composition, petrology, geochemistry, 14C terrestrial age and oxygen isotopes of the Shişr 033 CR chondrite. *Meteoritics & Planetary Science* **42**, 1581-1595 (2007).
45. H. S. Chan, Z. Martins, M. A. Sephton, Amino acid analyses of type 3 chondrites Colony, Ornans, Chainpur, and Bishunpur. *Meteoritics & Planetary Science* **47**, 1502-1516 (2012).

46. R. Hayatsu, E. Anders, in *Cosmo- and Geochemistry*. (Springer Berlin Heidelberg, 1981), vol. 99, chap. 1, pp. 1-37.
47. D. Yoshino, K. Hayatsu, E. Anders, Origin of organic matter in early solar system—III. Amino acids: Catalytic synthesis. *Geochimica et Cosmochimica Acta* **35**, 927-938 (1971).
48. S. Pizzarello, Catalytic syntheses of amino acids and their significance for nebular and planetary chemistry. *Meteoritics & Planetary Science* **47**, 1291-1296 (2012).
49. D. P. Glavin *et al.*, Unusual nonterrestrial l-proteinogenic amino acid excesses in the Tagish Lake meteorite. *Meteoritics & Planetary Science* **47**, 1347-1364 (2012).
50. A. S. Burton *et al.*, A propensity for n-ω-amino acids in thermally altered Antarctic meteorites. *Meteoritics & Planetary Science* **47**, 374-386 (2012).
51. A. S. Burton *et al.*, Amino acid analyses of R and CK chondrites. *Meteoritics & Planetary Science* **50**, 470-482 (2015).
52. M. Kuppers *et al.*, Localized sources of water vapour on the dwarf planet (1)[thinsp]Ceres. *Nature* **505**, 525-527 (2014).
53. L. Wilson, K. Keil, Clast sizes of ejecta from explosive eruptions on asteroids: implications for the fate of the basaltic products of differentiation. *Earth and Planetary Science Letters* **140**, 191-200 (1996).
54. Q. H. S. Chan, M. E. Zolensky, R. J. Bodnar, C. Farley, J. C. H. Cheung, Investigation of organo-carbonate associations in carbonaceous chondrites by Raman spectroscopy. *Geochimica et Cosmochimica Acta* **201**, 392-409 (2017).
55. A. Steele *et al.*, Comprehensive imaging and Raman spectroscopy of carbonate globules from Martian meteorite ALH 84001 and a terrestrial analogue from Svalbard. *Meteoritics & Planetary Science* **42**, 1549-1566 (2007).
56. A. L. D. Kilcoyne *et al.*, Interferometer-controlled scanning transmission X-ray microscopes at the Advanced Light Source. *Journal of Synchrotron Radiation* **10**, 125-136 (2003).
57. Y. Takeichi, N. Inami, H. Suga, K. Ono, Y. Takahashi, Development of a compact scanning transmission X-ray microscope (STXM) at the photon factory. *Chemistry Letters* **43**, 373-375 (2014).
58. Y. Takeichi *et al.*, Design and performance of a compact scanning transmission X-ray microscope at the Photon Factory. *Review of Scientific Instruments* **87**, 013704 (2016).
59. Jacobsen, Wirick, Flynn, Zimba, Soft X-ray spectroscopy from image sequences with sub-100 nm spatial resolution. *Journal of Microscopy* **197**, 173-184 (2000).
60. M. Ito, S. Messenger, Isotopic imaging of refractory inclusions in meteorites with the NanoSIMS 50L. *Applied Surface Science* **255**, 1446-1450 (2008).
61. R. Hagemann, G. Nief, E. Roth, Absolute isotopic scale for deuterium analysis of natural waters. Absolute D/H ratio for SMOW. *Tellus* **22**, 712-715 (1970).
62. H. Craig, The geochemistry of the stable carbon isotopes. *Geochimica et Cosmochimica Acta* **3**, 53-92 (1953).
63. A. Mariotti, Atmospheric nitrogen is a reliable standard for natural 15N abundance measurements. *Nature* **303**, 685-687 (1983).
64. D. P. Glavin *et al.*, Amino acid analyses of Antarctic CM2 meteorites using liquid chromatography–time of flight–mass spectrometry. *Meteoritics & Planetary Science* **41**, 889-902 (2006).
65. D. P. Glavin, J. P. Dworkin, Enrichment of the amino acid L-isovaline by aqueous alteration on CI and CM meteorite parent bodies. *PNAS* **106**, 5487-5492 (2009).

66. D. P. Glavin, M. P. Callahan, J. P. Dworkin, J. E. Elsila, The effects of parent body processes on amino acids in carbonaceous chondrites. *Meteoritics & Planetary Science* **45**, 1948-1972 (2010).

Acknowledgments

General: We thank Edwin Thompson and the National History Museum London for the Zag meteorite samples. We thank Simon Clemett for his help with acquiring data with the two-step laser mass spectrometer (L^2MS). We thank Aaron Burton for the use of UPLC-FD/QToF-MS facility. We acknowledge Sandra Pizzarello and Aaron Burton their helpful comments and suggestions provided on an earlier version of the manuscript. We acknowledge the careful and highly beneficial reviews by anonymous referees.

Funding: Q.H.S.C. acknowledges support from the NASA Postdoctoral Program at the JSC, administered by Universities Space Research Association through a contract with NASA. M.E.Z. was supported by the NASA Cosmochemistry Program. M.I. was supported ted by the JSPS Grants-in-Aid for Science Research (no. 26287142), the Shimadzu Science Foundation (2016) and the Astrobiology Center Program of National Institutes of Natural Sciences (NINS) (Grant no. AB261011, AB271007). Y.K. was supported by Japan Society for the Promotion of Science KAKENHI (grant number JP15K17794), the Astrobiology Center of National Institutes of Natural Sciences (grant number AB271015, AB281004), and The Mitsubishi Foundation. ALS beamline 5.3.2.2 is supported by the Director of the Office of Science, Department of Energy, under Contract No. DE-AC02-05CH11231.

Author contributions: Q.H.S.C. and M.E.Z. conceived and designed the project. M.E.Z. supervised the project. Q.H.S.C., M.F., and A.S. conducted the Raman analysis, and interpreted the L^2MS experimental data collected by Simon Clemett. Y.K., A.N., A.L.D.K., H.S., Y.T., Y.T. and K.M. performed the STXM-XANES experiments. M.I. conducted the NanoSIMS analyses. Q.H.S.C. conducted UPLC-FD/QToF-MS analyses. Q.H.S.C. and M.E.Z. prepared the meteorite, halite and amino acid samples, M.F. and M.E.Z. prepared the halite residue, and Z.R. prepared the FIB sections. Q.H.S.C., M.E.Z, Y.K., M.F., M.T. and A.S. analyzed the experimental data. Q.H.S.C., M.E.Z, Y.K., M.F., M.T. and A.S. contributed to the theory and interpretation of the results. All of the authors discussed the results and contributed to the writing of the manuscript.

Competing interests: The authors declare that they have no competing interests.

Data and materials availability: All data needed to evaluate the conclusions in the paper are present in the paper and/or the Supplementary Materials. Additional data related to this paper may be requested from the authors.

Figures and Tables

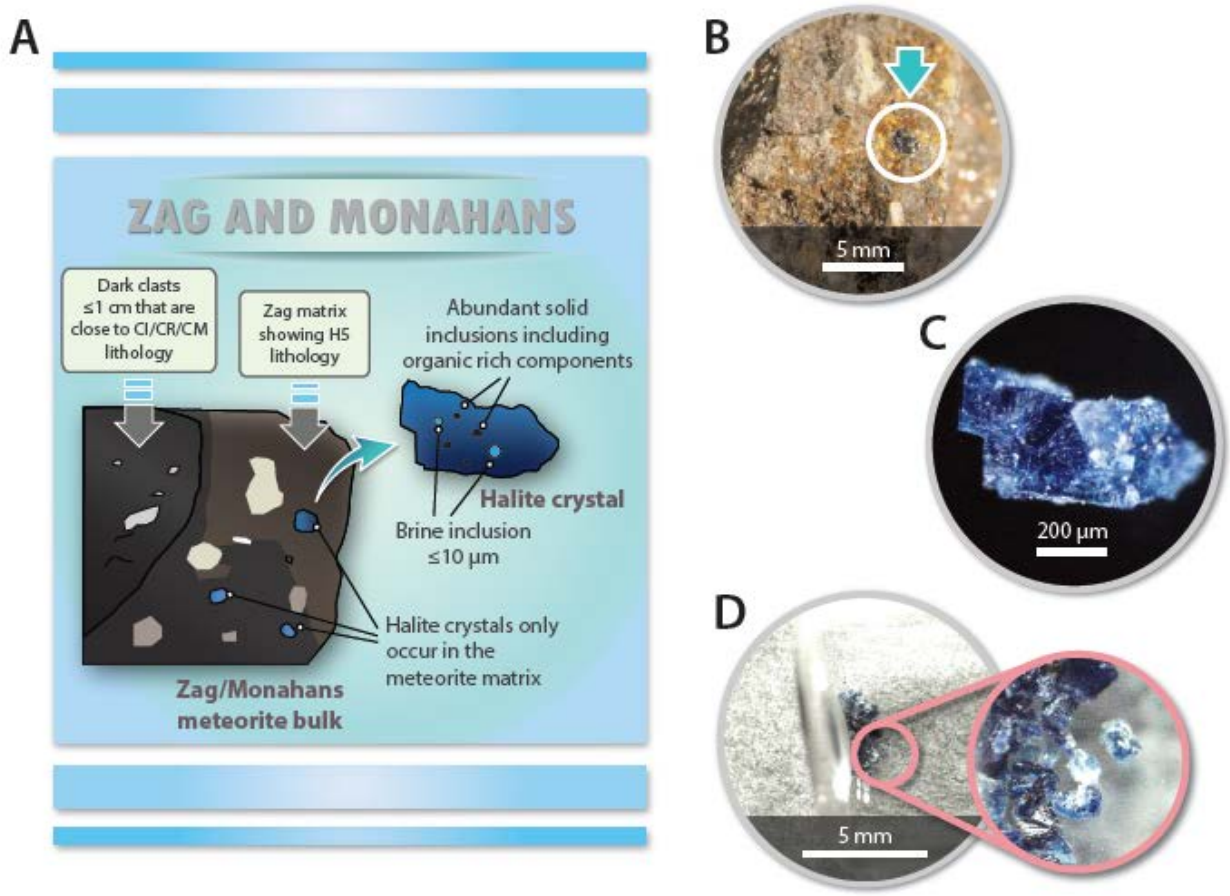

Fig. 1. Zag/Monahans meteorites and their halite crystals. (**A**) Illustration diagram showing the lithologies of the Zag and Monahans meteorites, their dark (carbonaceous) clasts, the halite crystals and the fluid and solid inclusions within the halite crystals. (**B**) Halite crystals hosted in the matrix regions of the Zag meteorite. The arrow marks one of the several halite crystals shown in this photo. (**C**) A microphotograph showing a halite crystal subsampled from the Zag meteorite. (**D**) Halite crystals subsampled from the Zag meteorite contained in a pre-sterilized glass ampoule prior to hot-water extraction.

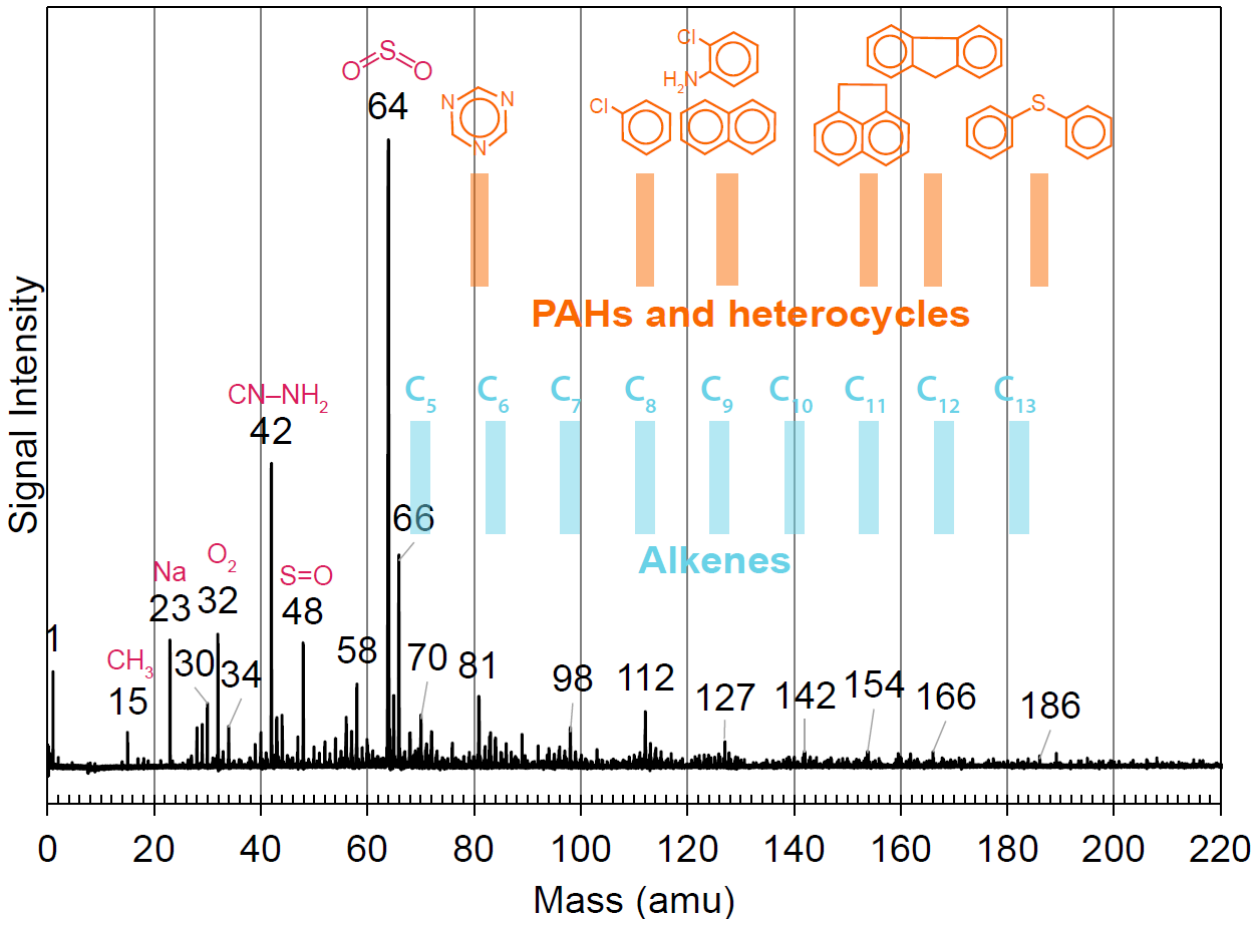

Fig. 2. μ-L^{2}MS spectra of the Zag halite. The y-axis of the spectrum is normalized to the largest peak for the range shown, represents a 36-shot average of the μ-L^{2}MS spectra. The chemical structures of the potential organic species are shown in orange (PAHs), blue (alkenes) and red (other lower mass molecules). The low-mass organics are comprised of derivatives and volatile species such as SO_2 (64 amu, and $^{34}SO_2$ at 66 amu) and its fragment SO at a lower abundance (48 amu). The spectrum is dominated by low-mass C_5–C_{10} hydrocarbons, such as alkenes (as shown by sequence of peaks separated by 14 amu), and PAHs/heterocycles such as triazine (81 amu), chlorobenzene (112 amu), chloroaniline (127 amu), naphthalene (128 amu), acenaphthene (154 amu) and fluorene (166 amu). The potential assignments of N-bearing compounds such as triazine and chloroaniline accounts for the odd-mass peaks.

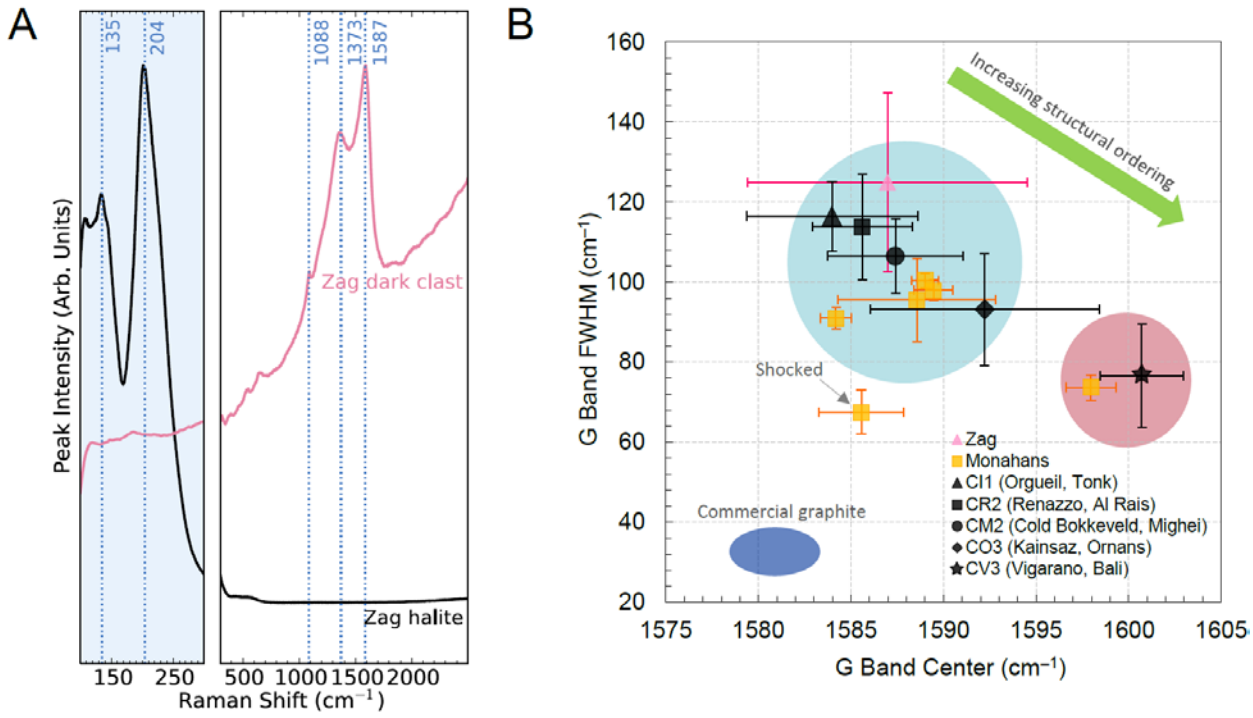

Fig. 3. Raman spectra and peak parameters of the halites and matrix in Zag and Monahans. (**A**) Representative Raman spectra (100–2300 cm^{-1} region) of the carbonaceous, halite-bearing clast (pink line) and halite grain (black line) of the Zag meteorite. The 100-300 cm^{-1} region of the plot has been expanded for clarity. Vertical lines mark the location of the typical Raman peaks of halite 135 cm^{-1} and 204 cm^{-1}, carbonate around 1088 cm^{-1}, and D and G bands around 1373 cm^{-1} and 1587 cm^{-1} respectively. (**B**) Raman G band spectral parameters of Zag matrix, Monahans halite residues, and carbonaceous chondrites hosted MMC. Several residue grains were collected from the same grain of Monahans halite and their Raman spectra parameters were expressed as individual points (yellow symbols). The black icons indicate a trend of MMC crystalline ordering in carbonaceous chondrites, from relatively poorly ordered CI chondrites to polycrystalline CV3 MMC. One grain of Monahans halite residue constitutes a single instance of MMC with affinity to CV3 chondrites (pink circle). Most MMC exhibits structural ordering similar to CI-CR-CM-CO chondrites (cyan circle), but one grain lies on a trendline between crystalline graphite and the main group. Thermal metamorphism does not drive ordering directly to graphite from disordered carbon, and spectra in this region are best explained as disordering of crystalline graphite, perhaps by shock. Overall, Monahans halite-hosted MMC is generally similar to CI-CR-CM-CO chondrites with minor input from CV3-like MMC and graphitic material that has been partially disordered. Error bars represent 1σ.

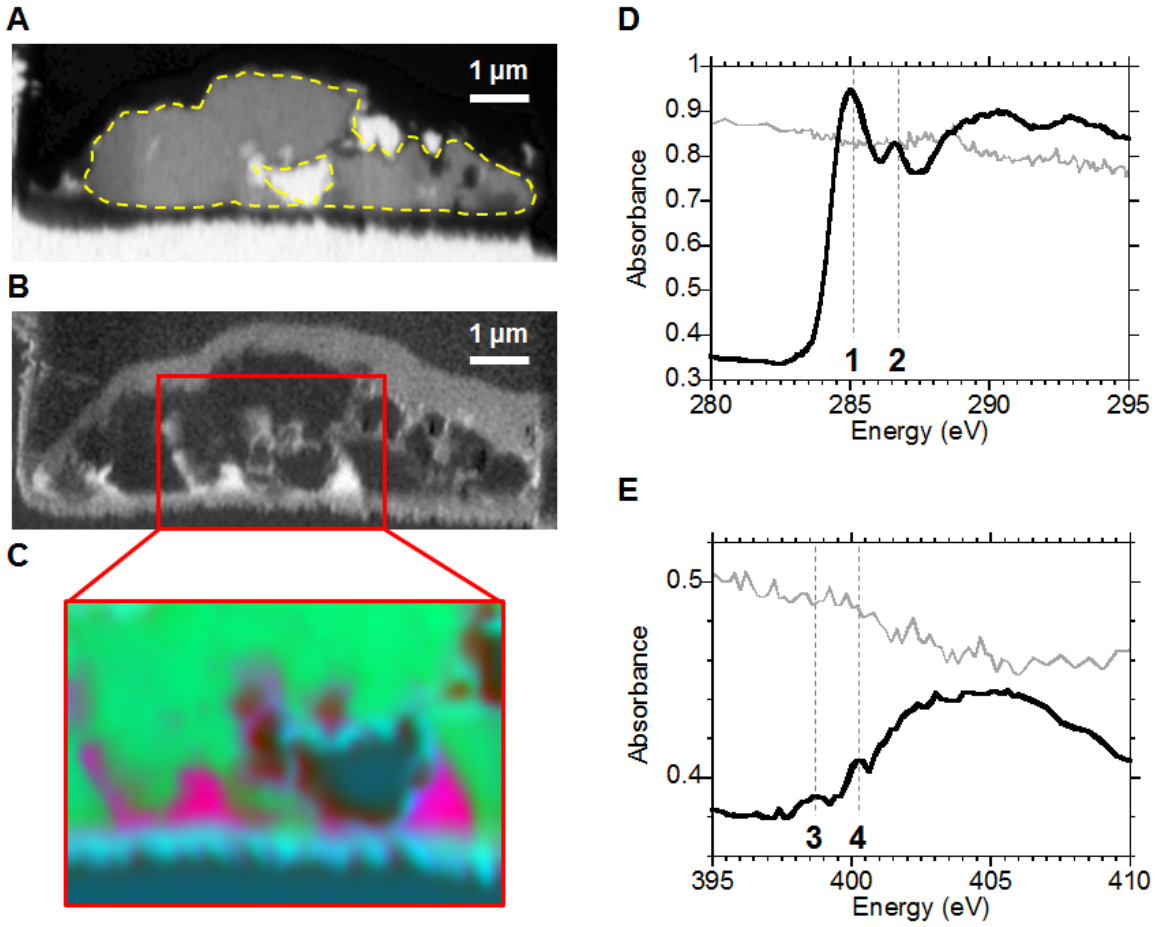

Fig. 4. STXM-XANES of the residue from halite in Monahans. (**A**) STXM single energy image at 390 eV refracting atomic density. Black indicates dense. (**B**) Carbon map obtained by taking the -log(I_{289}/I_{280}) for below (280 eV: I_{280}) and on (289 eV: I_{289}) the carbon *K*-edge. White indicates rich in carbon. (**C**) Spectral composed map. Red = Organic area, Green = Inorganic area, and Blue = Blank (e.g. holes). C-XANES spectra used to compose the RGB map are shown in **Fig. S3**. (**D**) C-XANES spectrum of organic areas (red areas in **Fig. 4C**) on the FIB section. Peak #1: 285.0 eV, 1s-π* of aromatic C. Peak #2: 286.6 eV, 1s-π* of ketone (C=O). C-XANES of Monahans meteorite matrix is also shown as thin line for comparison. (**E**) N-XANES spectrum of organic areas (red areas in **Fig. 4C**). Peak #3: 398.7 eV, 1s-π* of imine (C=N). Peak #4: 400.3 eV, 1s-π* of C=N in imidazole and/or protonated imine. N-XANES of Monahans meteorite matrix is also shown as thin line for comparison. The peak assignments of C,N-XANES are based on (*33, 68, 69*).

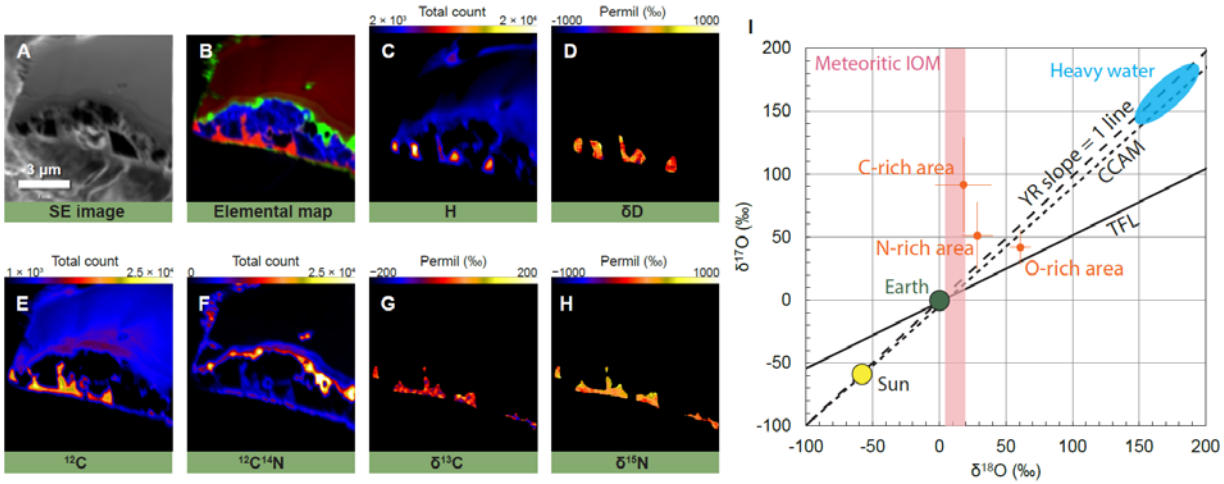

Fig. 5. Isotopic compositions of the Monahans halite residue. (**A**) SE image; (**B**) NanoSIMS elemental image, Red: C, Green: N, Blue: O, Field of View = 10 µm^2. The C-rich area (red) is well correlated with the organic area shown by STXM (red area in Fig. 4C). The green N-rich material appears to be contaminant as it can also be found outside the FIB section; (**C**) H, (**D**) isotope image of δD; (**E**) ^{12}C; (**F**) ^{12}C^{14}N – N is detected as the molecular CN^- ion due to the lower yield of N^- compared to CN^- under the Cs^+ beam; and isotope images of the C-rich region (**G**) δ^{13}C and (**H**) δ^{15}N. Scale bar is 3 µm. (**I**) O 3-isotope diagram comparing the oxygen isotopic compositions of the halite residue to that of other solar system materials. YR = Young & Russell; CCAM = carbonaceous chondrite anhydrous mineral; TFL = terrestrial fractionation line.

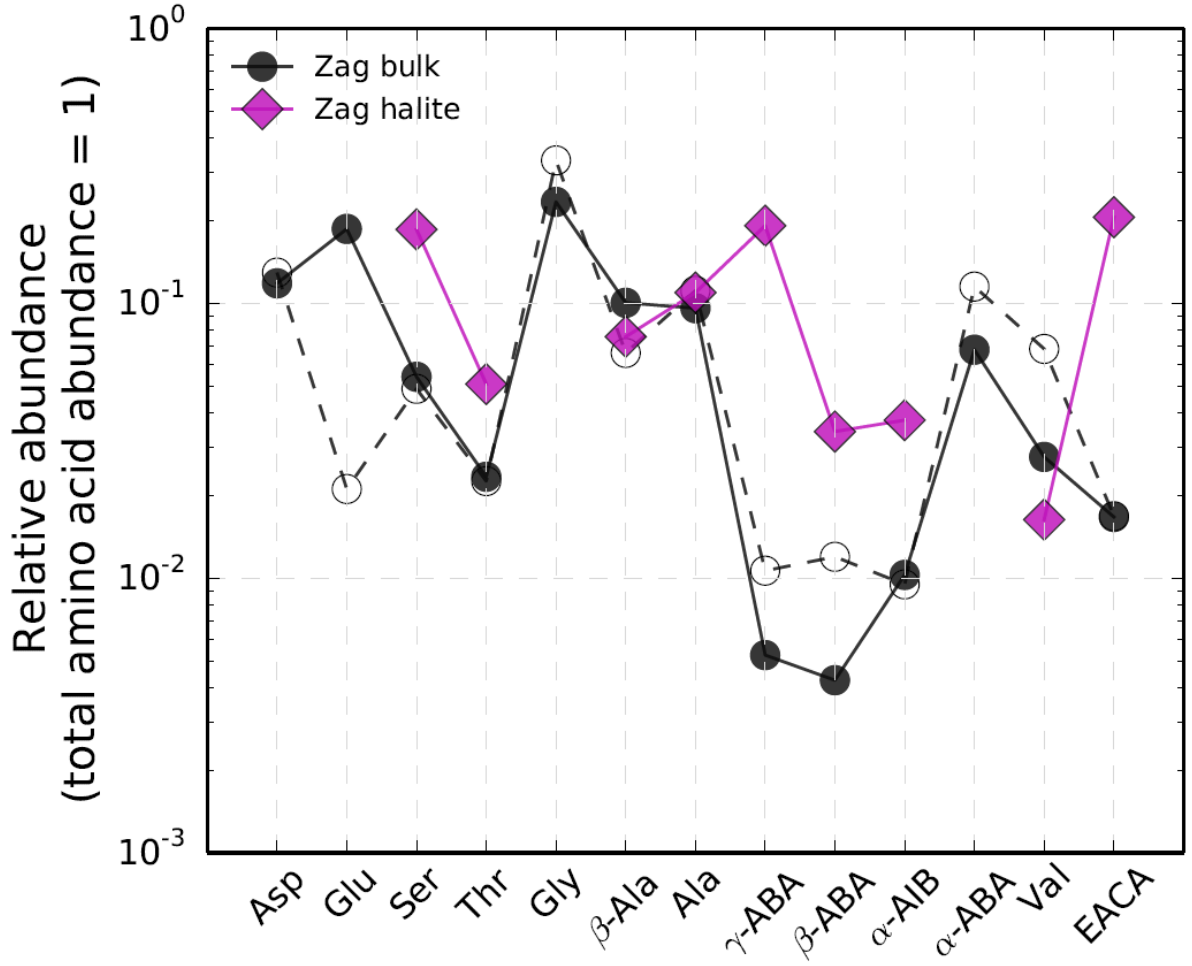

Fig. 6. Relative amino acid abundances (total amino acid abundance = 1) of the 6 M HCl acid-hydrolyzed amino acid extract of the Zag matrix (●), the non-hydrolyzed amino acid extract of the Zag matrix (❍), and the acid-hydrolyzed amino acid extract of the Zag halite (◆). While the Zag matrix is γ-ABA, β-ABA, α-AIB and EACA-deficient, the halite is shown to exhibit an opposite trend and is enriched in these amino acids. The striking difference in the amino acid contents between the halite and matrix indicates their separate synthetic origins. The abbreviations of the amino acids are defined in **Table S1**.

Table 1. Carbon, nitrogen, hydrogen and oxygen isotopic compositions of the C-rich and N-rich area in the halite residues of the Monahans meteorite. Errors are reported as 1σ. Isotopic data of CI, CM and CR chondrites and terrestrial organic matter are available in (*34*) and (*70*).

		Isotopic compositions (‰)				
Meteorite class	**Samples**	**$\delta^{13}C$**	**$\delta^{15}N$**	**δD**	**$\delta^{17}O$**	**$\delta^{18}O$**
H5	Monahans halite residues					
	C-rich area	−37.6 ± 4.6	+164.5 ± 14.4	+42.5 ± 54.3	+90.8 ± 37.1	+18.1 ± 20.9
	N-rich area	−56.1 ± 14.7	+106.1 ± 14.7		+50.5 ± 27.2	+28.1 ± 11.8
CI	Orgueil	−17.05 ± 0.04	+30.7 ± 0.2	+972 ± 2		+14.5 ± 0.6
CM	Murchison	−18.91 ± 0.01	−1.0 ± 0.4	+777 ± 27		+13.2 ± 0.6
CR	EET92042	−22.19 ± 0.1	+184.1 ± 1.4	3002 ± 12		+14.2 ± 0.3
CR (weathered)	El Djou	−23.18	44.5	223		+12.5
	Terrestrial organic matter	−60 to −25	−10 to +20	−350 to +50		